Journal of Biological Physics 31: 87–120, 2005.
DOI: 10.1007/s10867-005-1637-y

Dynamics of Bio-Polymeric Brushes Growing from a Cellular Membrane: Tentative Modelling of the Actin Turnover within an Adhesion Unit; the Podosome

THIERRY BIBEN[1,*], JEAN-CHRISTOPHE GÉMINARD[2] and FRANCISCO MELO[3]
[1]*Laboratoire de Spectometrie Physique, CNRS UMR 5588, Universite Joseph Fourier, 140 Avenue de la Physique, 38402 Saint Martin d'Heres, France;* [2]*Laboratoire de Physique, CNRS UMR 5672, Ecole Normale Superieure, 46 Allee d'Italie, 69364 Lyon Cedex 07, France;* [3]*Laboratorio de Fisica No Lineal, Universidad de Santiago de Chile Avenida Ecuador 3493, Casilla 307, Correo 2, Santiago (Chile)*
*(*Author for correspondence, e-mail: thierry.biben@ujf-grenoble.fr)*

Abstract. Podosomes are involved in the adhesion process of various cells to a solid substrate. They have been proven to consist of a dense actin core surrounded by an actin *cloud*. The podosomes, which nucleate when the cell comes in the vicinity of a substrate, contribute to link the membrane to the solid surface, but rather than frozen links, collective dynamical behaviors are experimentally observed. Depending on the differentiation stage, podosomes assemble and form clusters, rings or belts. Considering the dynamics of a polymeric brush, we design a simple model aiming at the description of a single podosome, the basic unit of these complex adhesion-structures and compare our theoretical conclusions to recent experimental results. Particularly, we explain, by solving the diffusion problem around the podosome, why the structure is likely to have a finite life-span.

Key words: polymeric brush, podosome, actin turnover

1. Introduction

All the adult life long, two types of cell insure the permanent renewal of the bone material: the *osteoclasts*, which resorb the bone, and the *osteoblasts*, which secrete new material replacing the old one. When an osteoclast encounters a substrate, small adhesion structures, the *podosomes*, appear in the contact region. Podosomes are local structures involved in the adhesion process of various cells (osteoclasts, macrophages, v-src-transformed cells) to a solid substrate [5–7, 10]. They have been proven to consist of a dense actin core surrounded by an actin *cloud* [2, 9].

In an initial stage of differentiation, the podosomes form aggregates (*clusters*) in which they remain randomly distributed with a distance of about 1.4 μm between

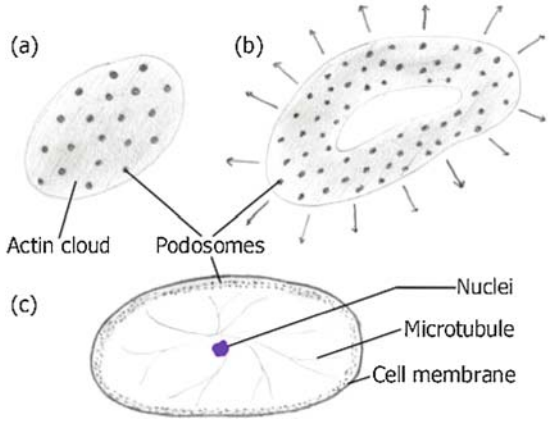

Figure 1. Diagrammatic behavior of the podosome structure: (a) Podosomes nucleate in the contact region between the cell membrane and the substrate. In this initial stage, they form a *cluster* in which they remain randomly distributed with a distance of about 1.4 μm between them. Within the *cluster*, they are surrounded by a diffuse actin cloud. (b) After typically 4-5 days of differentiation, podosomes disappear in the central region of the initial cluster. Podosomes then form a *ring* that migrates toward the periphery of the contact region. (c) In mature osteoclasts, when the ring reaches the cell periphery, a *belt* of podosomes, which then remains at rest, maintains the cell attached to the substrate [see [27] for biological details].

them (Figure 1a). In a second stage, podosomes disappear at the center of the initial cluster (after typically 4–5 days), forming then an annulus (*ring*) that migrates toward the periphery of the contact region, increasing then the surface area of the contact region between the cell and the substrate (Figure 1b). During this process podosomes preferably disappear (*die*) along the inner boundary of the annulus whereas they nucleate at the outer boundary, the resulting velocity of the structure toward the periphery of the contact region being roughly 2 μm.min^{-1}. In a final stage, in mature osteoclasts, when the structure reaches the periphery of the cell, the podosomes form a *belt* which maintains the cell anchored to the substrate (Figure 1c). In any of these three structures, the mean life-span of a single podosome is of about $\tau \simeq 2$ min while its growth time is around 30 s, as measured in photobleaching experiments [2]. Interestingly, an apparent steady state is thus observed during the life-span of the podosome that is suddenly interrupted, resulting in its death. Our scope here is to account for these experimental features.

In the confocal microscope, the apparent shape of a podosome is a cone of typical height $h = 0.5$ μm and base radius $r_p = 0.15$ μm. It is made of a dense assembly of actin filaments preferably oriented along the perpendicular to the cell membrane. FRAP (*Fluorescence Recovery After Photobleaching*) experiments have proven that podosomes are dynamical structures in spite of their stationary shape during their life-span [2]. The mechanisms that regulate these structures are not known at present but probably involve actin regulators that are specifically found in podosomes, like

cortactin and Wiskott-Aldrich syndrome protein (WASP), which localize directly underneath the podosome [9], and gelsolin, an actin severing agent essential for podosome regulation [1, 4]. Additional experiments indicate that the microtubules network is not necessary, at least in the two first stages of the adhesion process, while podosomes are in clusters or in an annulus [2]. The microtubule network seems to play an important role only during the last stage of differentiation, when podosomes form the belt that maintains the cell attached to the substrate.

In the present article, we focus on the dynamics of actin in the podosome and in the cloud. Reducing the complex biological system to a simplified model involving only the synthesis of actin filaments at the cell membrane and the severing, we account for the observed apparent shape of the single podosome and for the experimental FRAP results, which proved that podosomes are dynamical structures [2]. However, thanks to matter conservation, synthesis of the podosome requires that free monomeric species are present in the vicinity of the polymerization site. A self-consistent description of the dynamics thus requires a proper account of the diffusion of the molecular species involved in the synthesis and severing process. We show below that diffusion is responsible for the actin cloud formation and for the finite life-span of the podosome. The key ingredient is the competition between two characteristic time-scales: the relaxation time of the podosome dictated by the growing rate at the basis of the podosome competing with severing, and the relaxation time of the diffusing monomers. Indeed, whereas the growth of the podosome from its nucleation site is a local and relatively fast process, diffusion of the monomers across the system is slow in comparison. It can thus happen that the podosome reaches a quasi-steady state while the concentration profiles (and thus the cloud) are not yet equilibrated. Equilibration of the concentration profiles can result in a shortage of monomeric species at the basis of the podosome, causing its death.

The article is organized as follows: In Section 2, we present the model and the associated steady-state solutions while the dynamical response of the system is analyzed in Section 3. Finally, we discuss our theoretical results in regards to the experiments in Section 4.

2. Model and First Analysis

2.1. THE MODEL

We know from the experiments that each podosome consists of a set of actin filaments mainly oriented along the perpendicular to the cell membrane [2]. We assume that each of the filaments is connected to a nucleation site attached to the cell membrane (Figure 2) from which it grows by addition of actin monomers yet present in the cellular medium (*hyaloplasm*). From this point of view the dense core is thus simply a polymer brush growing from the substrate.

In the following $b_n(t)$ denotes the probability of finding a filament containing $(n+1)$ monomers in the podosome at time t (n is thus the number of bonds between

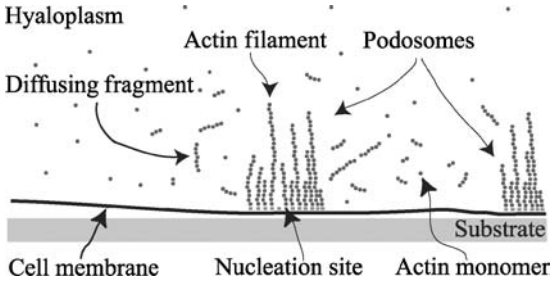

Figure 2. Sketch of the system. In our model, each podosome consists of a set of actin filaments, anchored at one end to a nucleation site and oriented mainly along the perpendicular to the cell membrane. The filaments grow from the cell membrane by addition of actin monomers yet present in the podosome region. The fragments cut from the podome diffuse freely in the hyaloplasm and form the actin cloud surrounding each podosome.

monomers). If M denotes the total number of nucleation sites in the podosome, $Mb_0(t)$ corresponds to the number of free nucleation sites (*i.e.*, the sites not occupied by any filament). In order to account for the growth of the polymer brush, we assume that one new actin-monomer is added at each nucleation site with the typical frequency, v. The resulting growth velocity of the existing filaments thus writes va, where $a = 2.7$ nm denotes the diameter of the actin monomer in the actin filaments [8]. The polymerization of the filaments thus induces an advection (propagation) of the distribution $b_n(t)$ toward larger values of n with the velocity v, which is likely to depend on the local concentration of actin monomers.

However, polymerization alone would induce a perpetual growth of the filaments, which is not consistent with the experimental observation of steady podosomes. Several limiting mechanisms are possible. The growth velocity v could be canceled after some time in order to produce a well-defined height of the structure above the cell membrane; the process would require an external signal from the nucleus, which has not been identified at present. Depolymerization of the actin filaments could occur at their free ends, leading thus to *treadmilling* (i.e. apparent translocation due to addition of monomers at one end and loss of monomers at the other end). However, such a depolymerization would not be compatible with the observation of actin-polymer fragments in the hyaloplasm around each podosome. Moreover, in the steady-state, the filaments disassembly would have to exactly counterbalance the filaments growth, which is very unstable. On the other hand, the gelsolin, experimentally found in the podosome structure, is known as a severing agent (this enzyme can cut the actin filaments at any polymer bond). As we will demonstrate in the following, the severing process can regulate naturally the filament length and account for the presence of free actin-polymers in solution within the podosome structure. Let us now assume that the density of the filaments within the brush is so large that the gelsolin can not diffuse within the structure, and then only cuts the filaments at the outer boundary of the structure (with the

typical frequency β). The resulting shape of the podosome would be a cone, which angle would be proportional to the ratio β/v. As a consequence, the height of the podosome (the cone) would be proportional to the radius of its base plane, which is not oberved experimentally. Moreover, in the confocal microscope, one can observe that the gelsolin does diffuse between the actin filaments [2]. Thus, we will assume that the polymeric chains are split at any bond with the typical frequency β, independent of the location within the podosome. Seeking for simplicity, we shall describe the activity of the severing agent by the frequency β only. We thus suppose that the concentration of the severing agent is constant and neglect any associated diffusion field. Moreover, we neglect the time the molecule is likely to remain attached to the actin filament and assume that the filaments are instantaneously cut when touched by the severing agent.

The two fundamental ingredients, polymerization at the nucleation site and severing, lead to the following equation for $b_n(t)$:

$$\frac{\partial b_n}{\partial t} = v\,[b_{n-1} - b_n] + \beta\left[\sum_{i=n+1}^{+\infty} b_i \; - n b_n\right] (\forall\, n \geq 0 \quad \text{with} \quad b_{-1} \equiv 0) \tag{1}$$

The v contribution expresses the growth at the nucleation site. The sum contains the information that any filament, which number of bonds is larger than n, can be split, with the typical frequency β, to provide a filament of number of bonds n [the situation corresponds to a filament cut at bond $(n+1)$, indexed from 0 at the nucleation site]. The last term $-\beta n b_n$ expresses the fact that the filament having n bonds can be attacked at any of its n bonds to give a smaller filament. This equation for b_n does not explicitly emphasize the coupling to the local concentration of the monomers, c_0, but this coupling is implicitly contained in v which can be a function of c_0 at the nucleation sites.

The fragments of the filaments cut from the brush diffuse freely in the hyaloplasm. While diffusing, they are themselves attacked by the depolymerization protein to produce smaller fragments. As a consequence, the actin concentration around the dense core of the podosome results from both the initial concentration of actin monomers in the hyaloplasm and the severing. Let us now denote $c_n(\mathbf{r}, t)$ the concentration of fragments containing $(n+1)$ monomers (thus n bonds) at position $\mathbf{r}$ and time t. The equation accounting for the diffusion and severing of the diffusing species outside the podosome can be written as:

$$\frac{\partial c_n(\mathbf{r})}{\partial t} = D_n \Delta_{\mathbf{r}} c_n(\mathbf{r}) + \beta\left[2\sum_{i=n+1}^{+\infty} c_i(\mathbf{r}) - n c_n(\mathbf{r})\right] \tag{2}$$

The first term, $D_n \Delta_{\mathbf{r}} c(\mathbf{r})$, accounts for the diffusion; D_n is the diffusion constant of a fragment containing $(n+1)$ monomers, and $\Delta_{\mathbf{r}}$ is the spatial Laplacian operator. A simple Einstein-like prescription [3] can be used to estimate D_n, namely that

the diffusion constant is inversely proportional to the polymer size; we take $D_n = D_0/(1+n)$, where $D_0 \simeq 30\ \mu\text{m}^2.\text{s}^{-1}$ [8] is the monomer diffusion constant. The second contribution, proportional to β, comes from the severing, and thus has the same structure as the corresponding term in Equation (1). The main difference is the factor 2; indeed the splitting of a single free fragment in solution produces two shorter free-fragments, whereas the splitting of a filament within the podosome leads to a shorter filament still belonging to the podosome, and only one free diffusing fragment. The boundary condition away from the isolated podosome, the cell being assumed to be infinitely large compared to the characteristic size of the diffusion fields, writes $c_n(\infty) = 0\ (\forall\ n > 0)$ and $c_0(\infty) = c_\infty$ associated to $\nabla c_n(\infty) = 0\ (\forall\ n \geq 0)$. On the other hand, the boundary condition at the podosome writes:

$$-D_n \int_S \nabla_{\mathbf{r}} c_n(\mathbf{r}) \cdot d\mathbf{S} = \left(\beta \sum_{i=n+1}^{+\infty} b_i - \delta_{n,0} v \sum_{i=0}^{+\infty} b_i \right) M \tag{3}$$

where S is a surface enclosing the podosome and $d\mathbf{S}$ is the normal outgoing surface element. M is the number of filaments in the podosome. This parameter can however be absorbed by a redefinition of c_n as will be done below. This equation simply expresses the conservation of matter at the surface of the podosome and accounts for the production of new free diffusing fragments as well as the consumption of monomers by the podosome. In the following, we shall consider S as an hemisphere of radius σ at which we shall apply the boundary condition, the spherical geometry allowing for an analytical solution for the concentration profiles. The radius σ thus represents the "typical size" of the podosome. In addition, we assume that σ is small compared to the typical diffusion length $\sqrt{D_0/\beta}$. In this approach, the podosome is therefore considered as a quasi point-like object (at the scale of the diffusion fields) located at the origin, $\mathbf{r} = \mathbf{0}$ (This assumption will be discussed in Section 4). While the first contribution, $\beta \sum_{i=n+1}^{+\infty} b_i$, is the density of fragments having n bonds released per unit time, the second contribution only acts on the monomer concentration $c_0(\mathbf{r})$ ($\delta_{n,0}$ is the Kronecker symbol), and accounts for the consumption of monomers at the nucleation sites.

2.2. THE STEADY STATE

Interestingly, Eqs. (1) and (2) can be solved analytically in the steady state. Equation (1) has a steady solution b_n^{st} that can be constructed by solving [from Eq. (1) with $\partial b_n/\partial t = 0$] :

$$b_{n-1}^{st} = b_n^{st} + \frac{\beta}{v}\left[n b_n^{st} - \sum_{i=n+1}^{+\infty} b_i^{st} \right]$$

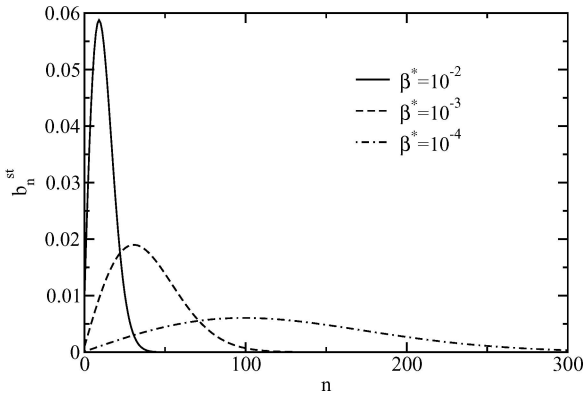

Figure 3. Steady distribution of filaments b_n^{st} vs. n for several β^*.

where v is associated to the steady concentration of monomers at the podosome $c_0(\sigma)$. One can check that the steady solution writes:

$$b_n^{st} = \frac{\beta^*(n+1)}{\prod_{i=0}^{n+1}(1+\beta^* i)} \tag{4}$$

where $\beta^* = \beta/v$ [Eq. (4) ensures the normalization $\sum_{n=0}^{+\infty} b_n^{st} = 1$]. We report in Figure 3 the steady distribution b_n^{st} for several values of β^*.

From Eq. (4), we can easily compute the average length of the filaments within the podosome in the steady regime, $\langle n+1\rangle \equiv \sum_{i=0}^{+\infty}(1+i)b_i^{st}$ [Figure 4, $\langle n+1\rangle$ stands for the average length in units of the monomer diameter, a]. One observes

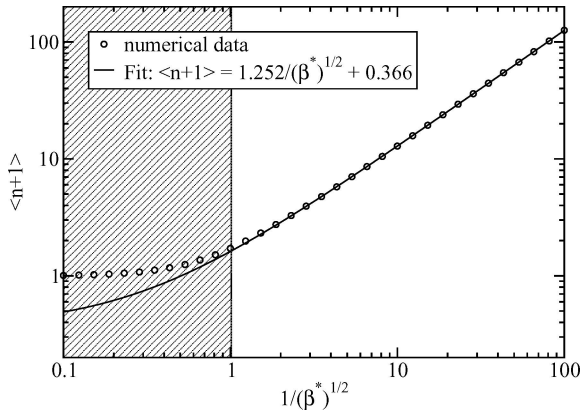

Figure 4. Average length $\langle n+1\rangle$ of the filaments as a function of β^*. For small values of β^*, $\langle n+1\rangle$ increases like $1/\sqrt{\beta^*}$. As expected, the average length of the filaments in the podosome increases when the polymerization velocity v is increased, and when the severing frequency β is decreased.

that $\langle n+1\rangle$ scales like $\sqrt{\pi/(2\beta^*)}$ for $\beta^* \ll 1$, showing that the characteristic size of a podosome diverges like $1/\sqrt{\beta^*}$ when β^* vanishes. Experimentally, the typical number of monomers in the filaments is of about $n = h/(2a) \simeq 100$, associated to $\beta^* \sim 10^{-4}$. In this limit, the discrete description of the filament distribution can be successfully replaced by the continuous description presented in the next Section 2.3.

The steady solution for the concentration fields can be obtained analytically as well (see Appendix I). Of particular interest is the monomer concentration field that will play a key role in the determination of the dynamical "phase diagram". Defining $\rho \equiv \sqrt{\beta/D_0}\, r$ where r is the distance to the podosome center, and $C_n(\rho) \equiv (D_0/\beta)^{3/2}\, c_n(r)/M$, the steady solution for the monomer concentration profile $C_0(\rho)$ expresses:

$$C_0(\rho) = \frac{C_\infty}{\beta^{*\frac{3}{2}}} - \frac{1}{2\pi(1+\sqrt{2}\rho_\sigma)}\,\frac{1}{\beta^*(1+\beta^*)}\,\frac{\exp[-\sqrt{2}(\rho-\rho_\sigma)]}{\rho} \tag{5}$$

with $\rho_\sigma \equiv \sqrt{\beta/D_0}\,\sigma$, $C_\infty = (D_0/v)^{\frac{3}{2}}\, c_0(\infty)/M$ and $c_0(\infty)$, the monomer concentration in the hyaloplasm far away from the podosome. Note that v (and thus β^*) is likely to depend on $C_0(\rho_\sigma)$ so that Eq. (5) has in general to be solved self-consistently to determine $C_0(\rho_\sigma)$ and the corresponding v (or β^*).

Before discussing these results, it is interesting to consider the limit $\beta^* \to 0$ which corresponds to the experimental situation where the typical length of the filaments within the podosome is much larger than the size of the monomeric units.

2.3. The continuous model in the limit $\beta^* \to 0$

The previous discrete model can be reformulated by considering n as a real variable when $\epsilon \equiv \sqrt{\beta^*} \to 0$. This statement can be justified by the fact that the average size of a podosome scales like $\langle n+1\rangle \propto 1/\epsilon$. In the limit $\beta^* \to 0$, the relevant variable is $x = \epsilon(n+1) \simeq n\epsilon$. Increasing n by 1 simply increases x by $dx = \epsilon$, a vanishingly small quantity. The full derivation is relegated to Appendix II but the general form of the equations can be guessed from (1) and (2), using the correspondence:

$$\begin{aligned} x &\leftrightarrow \sqrt{\beta^*}\, n \\ b(x) &\leftrightarrow b_n \big/ \sqrt{\beta^*} \\ c(x,r) &\leftrightarrow c_n(r) \big/ \sqrt{\beta^*} \end{aligned} \tag{6}$$

and the notations

$$\begin{aligned} t^* &= \sqrt{\beta v}\, t \\ r^* &= r \big/ \sqrt{D_0/v} \\ C(x,r^*) &= (D_0/v)^{\frac{3}{2}} c(x,r^*)/M \end{aligned} \tag{7}$$

Note that, with these conventions, $C(x, r^*)$ corresponds to $\beta^* C_n(\rho)$ for the discrete model. In the continuous limit, the equations write:

$$\frac{\partial b(x)}{\partial t^*} = \frac{\partial b(x)}{\partial x} + \int_x^{+\infty} b(y)\, dy \; - x b(x) \tag{8}$$

for the distribution, $b(x)$, of the actin filaments in the podosome, and:

$$\frac{\partial C(x, r^*)}{\partial t^*} = \frac{1}{x} \Delta_{\mathbf{r}^*} C(x, r^*) \; + 2 \int_x^{+\infty} C(y, r^*)\, dy - x C(x, r^*) \; (x > 0) \tag{9}$$

and the corresponding boundary condition at the podosome ($r^* = r_\sigma^* \equiv \sigma / \sqrt{D_0 / v}$)

$$-\frac{1}{x} \int_S \nabla_{\mathbf{r}^*} C(x, r^*) \cdot d\mathbf{S} = \int_x^{+\infty} b(y)\, dy \quad (x > 0) \tag{10}$$

for the concentration fields, $C(x, r^*)$, of the free diffusing fragments.

As for the discrete model, the stationary regime is obtained analytically as:

$$b^{st}(x) = x \exp\left(-\frac{x^2}{2}\right) \tag{11}$$

This solution again satisfies the normalization condition $\int_0^{+\infty} b^{st}(y)\, dy = 1$. We deduce from Eq. (11) that $\langle x \rangle = \sqrt{\pi/2}$. As a consequence, from Eq. (6), $\langle n + 1 \rangle \simeq \langle n \rangle = \sqrt{\pi / 2\beta^*}$, in agreement with the scaling proposed from the discrete model. The continuous description can be confronted directly with the discrete one, by rescaling both n and b_n by $\sqrt{\beta^*}$ and $1/\sqrt{\beta^*}$ respectively. Such a comparison is shown in Figure 5, and we observe a perfect agreement when β^* is lower than 10^{-2}.

The associated steady free-fragments concentration-profiles write:

$$C^{st}(x, r^*) = \left[1 - \frac{\left(r_\sigma^{*2} - 1\right)x - r_\sigma^* x^2}{(1 + r_\sigma^* x) r^*}\right] \frac{\exp[-x\,(r^* - r_\sigma^*) - x^2/2]}{2\pi (1 + r_\sigma^* x)}. \tag{12}$$

The monomer concentration field, which corresponds to $x = 0$, writes (see Appendix II):

$$C(0, r^*) \sim \frac{C_\infty}{\sqrt{\beta^*}} - \frac{1}{2\pi \sqrt{\beta^*}} \frac{1}{r^*} \exp[-\sqrt{2\beta^*}(r^* - r_\sigma^*)] \tag{13}$$

where $C_\infty = (D_0/v)^{\frac{3}{2}}\, c_0(\infty)/M$ is the dimensionless concentration of the monomers far away from the podosome. The result presented in Eq. (13), divided by β^*, compares to the monomer concentration obtained from the discrete model [Eq. (5)] at the leading order in β^* (please remember that $\rho^* = \sqrt{\beta^*} r^*$).

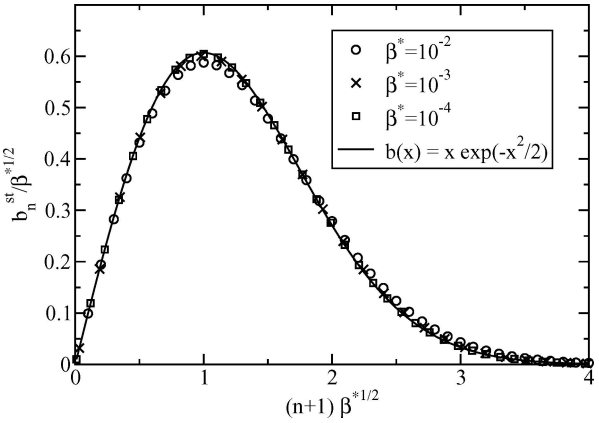

Figure 5. Comparison of the discrete and continuous models. The rescaled size-distribution b_n^{st} from figure 3 compare nicely with the asympotic form obtained within the continuous model framework [Eq. (11)].

In the next Section 3, we focus on the dynamical behaviors of the discrete and continuous models. The discussion in regards to the experiments will be presented in Section 4.

3. Dynamical Behaviors

The stationary solution, obtained analytically in Sections 2.2 and 2.3, is not always reached by the system. Indeed, the steady solution for the discrete and continuous models, exhibits a monomer concentration at the origin which is positive only if $C_\infty > 1/(2\pi r_\sigma^*)$, providing a first condition for the existence of a true steady-state. However, we will see that this criterion is too weak at finite β^* due to complex transient regimes; starting from an homogeneous concentration of monomers in the whole system, the monomer concentration in the vicinity of a growing podosome can vanish before the steady state is reached. In order to understand the phenomenon, it is important to distinguish the various relaxation times that appear in the problem. We first focus on the podosome and Eq. (1) which describes its growth. Then, we consider the entire problem, including the diffusion fields, and analyze the different dynamical regimes.

3.1. Growth of the podosome

The dynamics of the podosome growth is essentially controlled by the competition between polymerization at velocity v, assumed to be a constant in this part [this situation will indeed be useful to understand photobleaching data], and depolymerization at rate β, as illustrated by Eq. (1). The key control parameter is thus $\beta^* = \beta/v$ as already identified above.

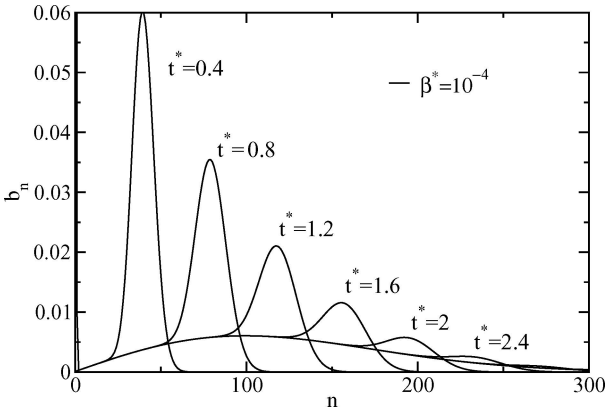

Figure 6. Distribution b_n at various times t^* during the podosome growth. One observes a large peak propagating toward increasing values of n at constant velocity v. For n located on the left-hand-side of the peak, the distribution $b_n(t)$ takes the steady value b_n^{st} ($\beta^* = 10^{-4}$).

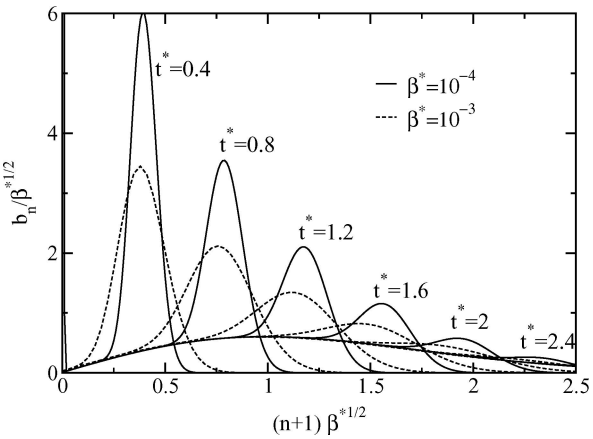

Figure 7. Rescaled distribution b_n at various times t^* for two values of β^*.

The dynamics of the relaxation to the steady state at constant polymerization frequency v can be followed numerically, starting from an initial state corresponding to monomeric species only ($b_0 = 1$ and $b_n = 0$ for $n > 0$) and solving Eq. (1). One typical result is shown in Figure 6. The large peak, that appears in the distribution $b_n(t)$, propagates at the velocity v toward increasing values of n. On the left-hand-side of the peak, the distribution $b_n(t)$ takes the values of the steady distribution b_n^{st}. The amplitude of the peak decreases while it propagates to ensure the normalization of the profile. Interestingly, rescaling the distribution profiles as done in Figure 5 allows to compare results obtained for different values of β^*. Such a comparison is presented in Figure 7: we observe that distributions b_n obtained for different values of β^* exhibit, for the same value of t^*, maximum values corresponding

almost to the same value of $(n+1)\sqrt{\beta^*}$. Thus, $1/\sqrt{\beta v}$ is truly the characteristic time of the podosome growth which justifies the choice of the dimensionless time $t^* \equiv \sqrt{\beta v}t$. In Figure 7, we also note that the width of the peak reduces with β^*. In the asymtotic regime $\beta^* \to 0$, this peak even becomes a δ distribution and, in this limit, the full analytical solution for $b(x, t^*)$ can be obtained as:

$$\begin{aligned} b(t^*, x) &= b^{st}(x) \quad \text{for } t^* > x \\ b(t^*, x) &= 0 \quad \text{for } t^* < x \\ b(t^*, t^*) &= \int_{t^*}^{+\infty} b^{st}(x)\, dx \end{aligned} \tag{14}$$

The proof that (14) satisfies (8) is relegated to Appendix III. Equation (14) is very helpful for determining the relaxation time, t^*_{relax}, of the distribution $b(t^*, x)$ to its steady-state value $b^{st}(x)$ which can be defined by

$$\left.\frac{\partial(\sqrt{\beta^*}\langle n\rangle)}{\partial t^*}\right|_{t^*=t^*_{\text{relax}}} = \epsilon_c$$

where ϵ_c is a cutoff. Reporting its value as a function of β^*, we find $t^*_{\text{relax}} \simeq 4$ corresponding to $t_{\text{relax}} \simeq 4/\sqrt{\beta v}$ (Figure 8). Thanks to equation (14), the average size of the podosome can be calculated at any time t^* as $\langle x\rangle = \int_0^{t^*} \exp(-x^2/2)\, dx$ from which we deduce $\partial\langle x\rangle/\partial t^* = \exp(-t^{*2}/2)$. The relaxation time is consequently $t^*_{\text{relax}} = \sqrt{-2\ \ln(\epsilon_c)}$ and depends only logarithmically on ϵ_c (Figure 8).

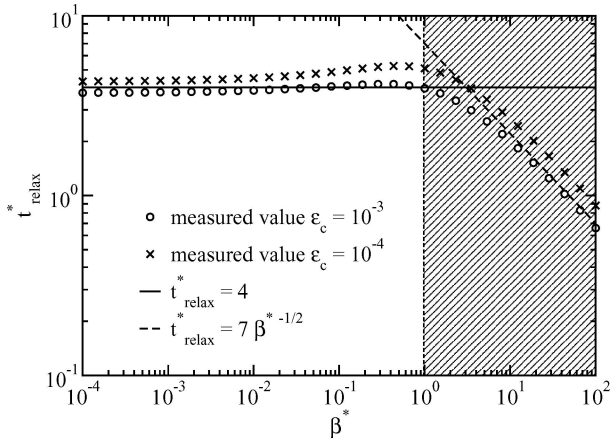

Figure 8. Relaxation time t^*_{relax} as a function of β^*. In the limit $\beta^* \ll 1$, which corresponds to the experimental situation, the podosome reaches its steady shape after the dimensionless time $t^*_{\text{relax}} \simeq 4$ corresponding to $t_{\text{relax}} \simeq 4/\sqrt{\beta v}$. We present the data for $\epsilon_c = 10^{-3}$ and 10^{-4}; the results are only slightly affected by the value of ϵ_c as can be checked in the $\beta^* \ll 1$ regime on the basis of the continuous model.

Thus, the characteristic time for the podosome to reach the steady state at constant polymerization velocity v and constant severing frequency β is expected to be $t_{\text{relax}} \sim 4/\sqrt{\beta v}$.

3.2. DEATH OF THE PODOSOME

Although we shall present later the dynamics of the concentration field, we anticipate here the possibility for the podosome to die while the filament distribution $b_n(t)$ has already reached its steady-state, due to a shortage of monomers in the medium. In such a case, the dynamics of the podosome can be obtained by setting v to zero in Eq. (1):

$$\frac{\partial b_n}{\partial \beta t} = \left[\sum_{i=n+1}^{+\infty} b_i \; - n b_n \right]$$

The only characteristic time that then remains in the problem is the severing time $1/\beta$. We thus expect the relevant variable for describing the death of the podosome to be βt rather than $t^* = \sqrt{\beta v}t$, where v stands for the polymerization velocity in the steady state before the shortage of monomers. Since we focus on the small β^* regime, this would imply the death to be much slower than the growth itself. We report in Figure 9 the variation of the characteristic height $\langle n+1 \rangle$ of a podosome during its growth, up to $t^* = 5$. At $t^* = 5$, we switch v to zero and monitor the decay of $\langle n+1 \rangle$. The relaxation is initially not exponential, as shown in Figure 10 where we plot $\langle n \rangle$ as a function of time in a semi-logarithmic representation. However

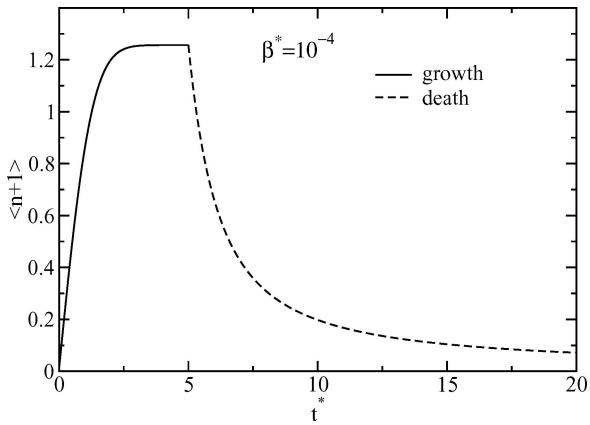

Figure 9. Growth-death sequence of a podosome ($\beta^* = 10^{-4}$). We observe the rapid variation of the characteristic height $\langle n+1 \rangle$ of a podosome during its growth, up to $t^* = 5$. At $t^* = 5$, we set v to zero. We observe the initial rapid decrease of the podosome height for $t^* > 5$ followed by a slower exponential decay at long times.

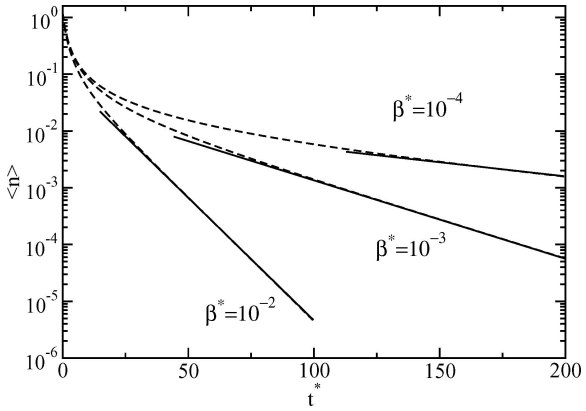

Figure 10. Semi-logarithmic plot of $\langle n \rangle$ as a function of time. We observe an exponential decay, corresponding to $\langle n \rangle \propto \exp(-\sqrt{\beta^* t^*})$, only at long times.

an exponential behavior with a characteristic time $1/\beta$ is observed at long times (the full curves). The situation at short times can easily be understood since we initially start from a steady configuration where the severing contribution [the term proportional to β in equation (1)] compensates exactly the growth term proportional to v. The severing term is thus equal, in the steady regime, to an advection term at velocity $-v$. As a consequence, when growth is suddenly cancelled, the early stage of the decay corresponds to a backward advection of the profile at a velocity $-v$. We report in Figure 11 the typical evolution of the distribution $b_n(t)$ as a function of time during the podosome death. Note in Figure 9 that the height of the podosome decreases by a factor 2 mainly in the initial almost linear regime. As a consequence, the typical initial height of the podosome being $\sqrt{\pi/2\beta^*}$ in the stationary regime,

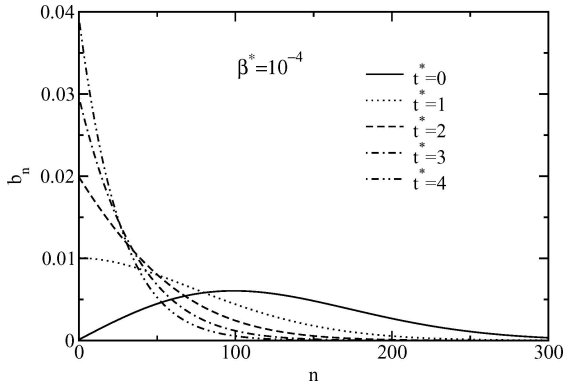

Figure 11. Evolution of the distribution $b_n(t)$ during the death of the podosome. The distribution first relaxes in an advective way (propagation) at velocity $-v$. However, since a pure propagative backward relaxation is not compatible with the presence of the boundary in $n = 0$, the decay becomes exponential with a characteristic time $1/\beta$ quite rapidly.

we can estimate the typical time t_{death} for the severing agent to release the podosome: $t_{\text{death}} \sim \sqrt{\pi/2\beta^*}/v = \sqrt{\pi/32}t_{\text{relax}}$.

The characteristic time t_{death}, for the severing agent to release the stationary podosome when the polymerisation velocity v suddenly cancels, equals, within a numerical factor of the order of unity, the relaxation time t_{relax}. Thus, the typical times for growth and death of the podosome both scale like $1/\sqrt{\beta v}$.

3.3. THE DYNAMICAL REGIMES

The dynamical behavior of the freely diffusing species can not be obtained as simply as the growth of the podosome since the coupling between the diffusing fragments and the podosome appears explicitly in Eq. (2). We thus need to solve the whole set of equations. Seeking for simplicity, we assume that the polymerization velocity v is constant when monomers are present in the vicinity of the podosome, and cancels when their concentration $C_0(r_\sigma^*, t^*)$ reaches zero. We will further assume that once the velocity has been canceled, the growth does not restart and the podosome dies due to the depolymerization process (Section 3.2). The model we consider here is thus a two-state model, $v = 0$ or $v \neq 0$. Such a model can be viewed as a limiting case where we have an excess of actin monomers in the cell. Indeed, the general dependence we can expect for v as a function of the monomer concentration c_0 is a linear dependence at low concentration, thanks to the linear response theory, and a saturation above a certain concentration threshold c_0^{sat}. A simple ansatz for $v(c_0)$ would thus be $v \propto \tanh(c_0/c_0^{\text{sat}})$. We consider here the situation where $c_0^{\text{sat}} \ll c_\infty$, the initial value of c_0, for which the hyperbolic tangent reduces to a step function.

We again restrict the discussion in this section to the limit $\beta^* \ll 1$, which corresponds to the experimental situation. The dynamical "phase diagram", which describes the possibility for the system to reach the steady state, depends strongly on the possible cancellation of the monomer concentration at the podosome, $C_0(r_\sigma^*, t^*)$, during the transient regime. In the stationary regime, we have seen that this cancellation is governed by the parameter C_∞ related to the monomer concentration in the cell far away from the podosome. We will thus investigate the dynamical phase diagram by varying this parameter. It is clear that the equilibrium steady-state is reached after some time (t_{relax}^* for the relaxation of the podosome, and usually a longer time for the relaxation of the concentration fields) when the monomer concentration in the cell is "very large". By contrast, if the monomer concentration in the cell is "very low", the depletion of the monomers around the podosome leads to a cancellation of the monomer concentration at the podosome after a time t_{life}^*, leading to the death of the podosome. Thus, depending on the relative values of t_{life}^* and t_{relax}^*, different dynamical behaviors are expected.

We already know that $t_{\text{relax}}^* \simeq 4$ (Section 3.1). We now need to estimate t_{life}^* and to check how the transition between finite and infinite values of t_{life}^* occurs.

We solve numerically Eqs. (1) and (2) starting from the initial condition $b_n = \delta_{n,0}$ and $C_n(r) = C_\infty \delta_{n,0}$ corresponding to a homogeneous distribution of monomers in the cell and a vanishingly small podosome. Thanks to the linearity of the model, a variation of C_∞ simply shifts the monomer-concentration profile $C_0(r^*, t^*)$ by the same amount. The constant C_∞ thus contributes to $C_0(r^*, t^*)$ in a trivial way, i.e. as an additive constant. It is then interesting to extract this quantity from the monomer-concentration profile and write, thanks to the superposition principle:

$$C_0(r^*, t^*) = C_\infty + C_0^v(r^*, t^*) + C_0^\beta(r^*, t^*) \tag{15}$$

where $C_0^v(r^*, t^*)$ accounts for the feeding of the podosome at its basis [the "v" term in Eq. (3)] while $C_0^\beta(r^*, t^*)$ accounts for the severing process [the "β" term in Eq. (3)]. Since C_∞ is accounted apart, both $C_0^v(r^*, t^*)$ and $C_0^\beta(r^*, t^*)$ cancel at $t^* = 0$. To investigate the variations of these two functions, a value of C_∞ can be chosen arbitrarily. We used $C_\infty = 0.2$ [$C_\infty = (v/D_0)^{\frac{3}{2}} c_0(\infty)/M$ is a dimensionless quantity], a large enough value that allows the podosome to reach the steady regime [One must note that $C_0(r^*, t^*)$ corresponds to $\beta^{*\frac{3}{2}} C_0(\rho, t^*)$ for the discrete model and thus to $\sqrt{\beta^*} C(x = 0, r^*, t^*)$ for the continuous model, so that C_∞ appears without any $\sqrt{\beta^*}$ in front of it in Eq. (15)].

Let us first monitor in Figure 12 the overall variation of the monomer concentration at the basis of the podosome for various values of β^*. We observe many interesting features: the value of β^* does not affect the decay at short times, a minimum appears at finite time, and the relaxation to the asymptotic value at long times explicitly depends on β^*. The last β^*-dependence is not surprizing since the

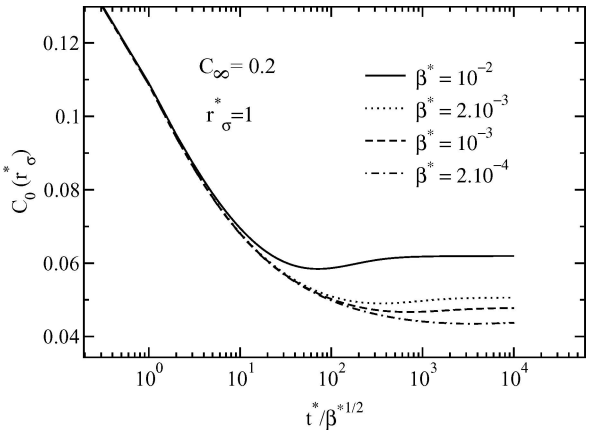

Figure 12. Time-evolution of the monomer concentration $C_0(r_\sigma^*)$ at the podosome.

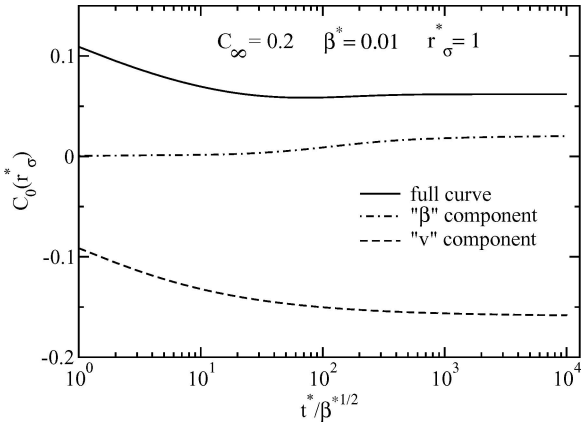

Figure 13. Time-evolution of $C_0(r_\sigma^*)$ and components C_0^v and C_0^β ($\beta^* = 10^{-2}$).

asymptotic value that can be obtained from the analytical steady solution (5)

$$C_0(r_\sigma^*) = C_\infty - \frac{1}{2\pi r_\sigma^*(1+\sqrt{2\beta^*}r_\sigma^*)(1+\beta^*)} \tag{16}$$

explicitly depends on β^*.

Although an exact description of the temporal evolution is not available yet, the suggested separation (15) makes it possible to better understand the relaxation process and to write an approximate expression. Figure 13 shows the two components, C_0^v and C_0^β for $\beta^* = 0.01$. We can see that, while C_0^v expresses the monomer consumption at the basis of the podosome and thus results in a decay of the monomer concentration, C_0^β accounts on the contrary for the monomer production due to severing and thus results in a growth of the monomer concentration. Since the monomer consumption is fixed by the frequency v, C_0^v does not explicitly depend on β^*, whereas the severing process does. Since severing is very slow compared to the polymerization process, C_0^β only acts at long times leading to the complex behavior observed in Figure 12. To go further, an approximate expression can be suggested for C_0^v:

$$C_0^v(r_\sigma^*) \simeq -\frac{1}{2\pi r_\sigma^*}\left[1 - \frac{1}{1+\left(\gamma\ t^*/\left[\sqrt{\beta^*}r_\sigma^{*2}\right]\right)^\alpha}\right] \tag{17}$$

where the prefactor $1/(2\pi r_\sigma^*)$ can be obtained analytically in the asymptotic regime, and the two parameters "γ" and "α" have to be determined numerically. We would expect $\alpha = 1/2$ and $\gamma = \pi$ from a diffusion process but, although these two values provide an excellent approximation at long times, they do not provide the best fit

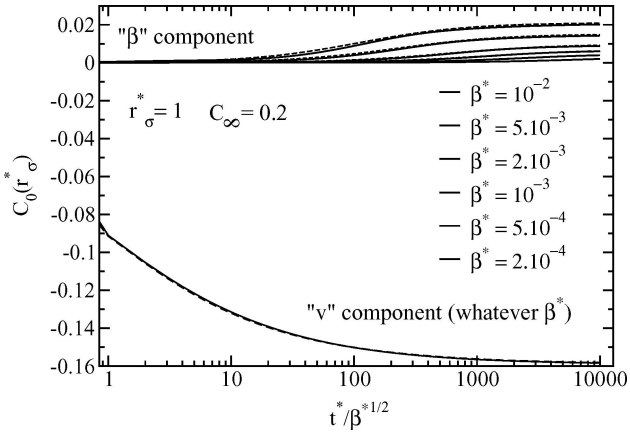

Figure 14. Time-evolution of C_0^v (dashed line) and C_0^β (full lines). While C_0^v is unsensitive to β^*, C_0^β varies significantly. From top to bottom C_0^β curves correspond respectively to $\beta^* = 10^{-2}$, $5.10^{-3}, 2.10^{-3}, 10^{-3}, 5.10^{-4}, 2.10^{-4}$. Superimposed to each of these curves are the approximate expressions presented in the text (thin dashes for C_0^β and the thin full line for C_0^v). The agreement is so good that these lines are barely visible, they can be seen for $\beta^* = 10^{-2}$.

given by $\alpha = 0.55$ and $\gamma = 1.7$. The second contribution C_0^β can be rewritten as:

$$C_0^\beta(r_\sigma^*) = bf(\beta^*, r_\sigma^*, t^*) \tag{18}$$

where f is a function varying between 0 (at $t^* = 0$) and 1 (at $t^* = \infty$). The prefactor b can be obtained analytically from the asymptotic steady solution as:

$$b = \frac{1}{2\pi r_\sigma^*}\left[1 - \frac{1}{(1+\sqrt{2\beta^*}r_\sigma^*)(1+\beta^*)}\right] \tag{19}$$

When $r_\sigma^* = 1$, f can further be approximated by $f \simeq 1 - 1/(1+\sqrt{\beta^*}t^*)$, but the r_σ^* dependence is quite complicated in general. In Figure 14, our approximate solutions exhibit very good agreement with the numerical data.

The dynamical phase-diagram can be obtained from these results quite easily. First it must be noted that the criterion for the existence of a stationary podosome based on the positivity of the steady solution (5) is insufficiant since the decay of the monomer concentration at the podosome is non-monotonic. Rather, while β^* is varying, we can see from Figure 12 that $C_\infty + C_0^v$ is the envelope of the minimal values reached by the concentration at the podosome. In the small β^* regime, we can thus expect the life span of a podosome to be given by $C_\infty = -C_0^v$. Inserting (17) in this criterion, we get:

$$\frac{t_{\text{life}}^*}{\sqrt{\beta^*}r_\sigma^{*2}} = \frac{1}{\gamma}\left(\frac{2\pi r_\sigma^* C_\infty}{1 - 2\pi r_\sigma^* C_\infty}\right)^{1/\alpha} \tag{20}$$

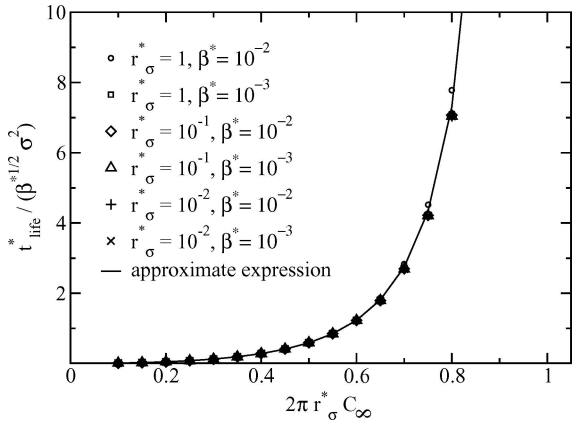

Figure 15. Life-span t^*_{life} of the podosome: comparison between the approximated expression and the numerical findings for various values of β^* and r^*_σ. Agreement is excellent even close to the critical concentration $2\pi C_\infty = 1$ (not shown here).

where $\gamma \simeq 1.7$ and $\alpha \simeq 0.55$. This expression can again be compared to the numerical data for various values of β^* and r^*_σ, as shown in Figure 15. We can note that the typical size r^*_σ of the podosome is not a crucial parameter since it only plays a role in combination with other parameters, in particular with C_∞. A pole exists in Eq. (20) at $2\pi r^*_\sigma C_\infty = 1$, which is precisely the steady criterion provided by the continuous model in the $\beta^* \to 0$ regime. This is not a surprise since in this asymptotic regime, C_0^β vanishes ($b = 0$), and thus the minimum observed in the concentration profile $C_0(r^*_\sigma)$ disappears (Figure 12).

We conclude from this study that the podosome can reach the steady state and exist forever provided that $2\pi r^*_\sigma C_\infty > 1$. When $2\pi r^*_\sigma C_\infty < 1$ the podosome life-span is approximatively given by equation (20) in the small β^* regime. Two situations can then occur: if $t^*_{\text{life}} > t^*_{\text{relax}}$, the podosome reaches a transient steady-state at t^*_{relax} and dies after t^*_{life}. If $t^*_{\text{life}} < t^*_{\text{relax}}$, the podosome disappears before reaching a steady shape. Since the relaxation time is estimated to be around $t^*_{\text{relax}} = 4$, expression (20) can be inverted to give the transient steady line:

$$2\pi r^*_\sigma C^{\text{trans}}_\infty = 1 - \frac{1}{1 + \left[4\gamma / \left(\sqrt{\beta^*} r^{*2}_\sigma\right)\right]^\alpha} \tag{21}$$

with $\gamma \simeq 1.7$ and $\alpha \simeq 0.55$. We can note on this expression that for small values of β^*, $2\pi r^*_\sigma C^{\text{trans}}_\infty$ goes to one, and thus the transient steady region becomes very narrow for the podosome. The dynamical phase diagram thus exhibits three different regions which can be described as follows in the small β^* regime:

- $2\pi r^*_\sigma C_\infty < 2\pi r^*_\sigma C^{\text{trans}}_\infty$, the podosome dies before reaching its steady state, the monomer concentration is too low in the system to generate a steady podosome.

- $2\pi r_\sigma^* C_\infty^{\text{trans}} < 2\pi r_\sigma^* C_\infty < 1$, the podosome reaches a transient steady-state, but dies after a time t_{life}^* given by expression (20).
- $1 < 2\pi r_\sigma^* C_\infty$, the steady state is reached for both the podosome and the diffusion field. The podosome remains indefinitely stable.

When β^* is not vanishingly small, the last criterion has to be slightly modified to account for the presence of a minimum in the monomer-density relaxation-profile at the podosome.

We point out that the model thus accounts for one important qualitative feature of the experimental observations: the podosome can exhibit a stationary shape during a finite life-span. The system only requires the condition $1 - 1/\{1 + [4\gamma/(\sqrt{\beta^*} r_\sigma^{*2})]^\alpha\} < 2\pi r_\sigma^* C_\infty < 1$ to be satisfied ($\gamma = 1.7$ and $\alpha = 0.55$). In the following section, we will show that the model also accounts for the observations in the confocal microscope and for the FRAP experiments.

4. Confocal Microscopy and Photo-Bleaching Experiments

The dynamics of a podosome can be probed experimentally using fluorescent markers (Actin-GFP, for instance). Experimental imaging in the confocal microscope and FRAP experiments have been succesfully used to investigate the structure of the podosomes and their dynamics. We dedicate this section to the comparison between our theoretical description of the system and the experimental results obtained by Destaing *et al.* [2].

4.1. The shape of a podosome in the confocal microscope

Confocal microscopy gives access to the local fluorescent intensity $I(z)$ in a slice of thickness dz located at a given distance z from the substrate. Due to the principle of the confocal microscopy, in the considered experimental conditions [Microscope: Carl Zeis, LSM 510, Magnification: 63×, Aperture: 1.4] dz is of about the wavelength $\lambda = 488$ nm of the fluorescent light and the spatial resolution ϕ in the observation plane of about $\lambda/2$. In osteoclasts, the apparent shape of a podosome is a cone of height $h \sim 0.5$ μm and radius at the basis $r_p \sim 0.15$ μm (Note that the radius r_p is smaller than the in-plane resolution ϕ).

We can easily extract the "expected" apparent shape of the podosome from the distribution b_n^{st} (Section 2), if we assume that the polymeric brush is made of rigid polymers oriented along the perpendicular to the planar substrate. Indeed, in such a situation the distance z between a monomer and the substrate is simply proportional to its index n in the chain. Let us thus express the distance z in monomeric units a. As $r_p < \phi$, a podosome appears like a bright dot in the image from the confocal microscope. The local fluorescent intensity measured at a given altitude $z^* = z/a$ is proportional to the number of the filaments cut by the observation

plane:

$$I(z^*) \propto \sum_{n \geq z^*}^{+\infty} b_n \tag{22}$$

In Eq. (22), we assume that the thickness $dz = a$ of the confocal slice is much less than the total height h of the podosome. However, if necessary, Eq. (22) can be replaced by:

$$I(z^*) \propto \int_{z^* - \frac{dz}{2a}}^{z^* + \frac{dz}{2a}} \left(\sum_{n \geq y}^{+\infty} b_n \right) dy \tag{23}$$

Since intensity $I(z^*)$ is proportional to the number of the filaments cut by the observation plane at a distance z^* from the substrate, we can define an effective radius $r \propto \sqrt{I(z)}$ in order to account for the apparent radius of the podosome at height z. The "expected" apparent shape of the podosome obtained from the discrete model resembles a cone (Figure 16), which height $h^* \equiv \sqrt{\beta^*} h/a$ is easily obtained from the continuous model. Indeed, from Eq. (11), the intensity $I(x)$ writes:

$$I(x) = \int_x^{+\infty} b^{st}(y)\, dy = \exp(-x^2/2) \tag{24}$$

where $x = \sqrt{\beta^*} z^*$.

Several prescriptions can be used to define h^*; The inflection point of the profile is located at $r = \exp(-1/2)$, corresponding to $x = \sqrt{2}$, the tangent at this point being given by $x = \sqrt{2}\,[2 - r\ \exp(1/2)]$. We can define h^* as the height of the cone formed by the tangents, so that $h^* = 2\sqrt{2}$.

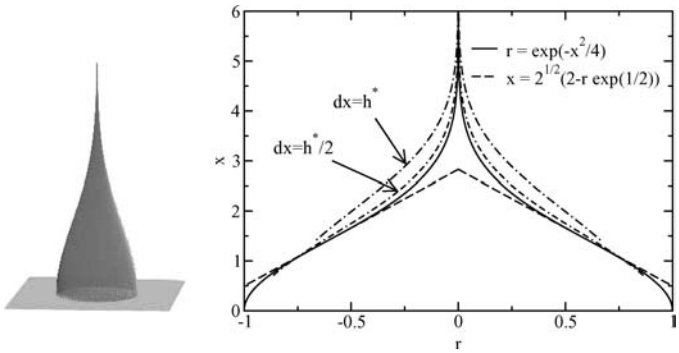

Figure 16. Apparent shape of the podosome in the confocal microscope. Left-hand side: 3D representation of the "apparent" shape of a podosome (for $dx = 0$). Right-hand side: Profile $x(r)$ (we take arbitrarely $r_p = 1$). Several values for the confocal thickness dx are presented, ranging from $dx = 0$ (the full curve) to $dx = h^*$.

Thus, the apparent shape of a podosome in the confocal microscope is a cone of height $h = 2\sqrt{2/\beta^*}a$. Note that, taking into account the thickness dz (or the corresponding dx in the continuous model) of the confocal slice does not change significantly the predicted apparent-shape (Figure 16). However, we point out that the model does not allow to predict the radius r_p which is likely to be given by the distribution of the nucleation sites from which the podosome grows.

4.2. FRAP EXPERIMENTS

Photo-bleaching a podosome corresponds to the destruction of the fluorescent properties of the monomers present in it thanks to an intense source of light. We point out that the structure is not affected by the process, only the optical activity of the fluorescent dye is altered in the bleached region. After bleaching, new fluorescent monomers, diffusing freely from outside of the bleached region, are incorporated at the basis of the podosome and fluorescence of the dense core is restored after some time. If we assume that diffusion of the monomeric species in the solution is fast compared to the growth process of the podosome, we can consider that the monomeric species included at the basis of the podosome are all fluorescent.

We can obtain, from the discrete model, an analytical expression for the recovery of the global fluorescence intensity $I = \sum_{n=0}^{+\infty} I_n(t)$, where $I_n(t)$ is the fluorescence intensity at altitude n, and time t when vt is an integer. Since the recovery of fluorescence comes from the incorporation of fluorescent monomers at the basis of the podosome, $I_n(t) = 0$ if $n > vt$ and $I_n(t) = \sum_{i=n}^{+\infty} b_i^{st}$ otherwise. Here, b_i^{st} is the steady distribution of polymers containing i monomers (fluorescent or not) in the podosome. This expression simply expresses that the steady structure of the podosome is repopulated with fluorescent monomers at a constant velocity v from the basis of the podosome. The global fluorescent intensity thus writes:

$$I^{\text{discrete}}(t) = \sum_{n=0}^{+\infty} I_n(t) = \sum_{n=0}^{vt} I_n^{st} = \sum_{n=0}^{vt} \sum_{i=n}^{+\infty} b_i^{st} \tag{25}$$

where I_n^{st} is the steady intensity at altitude n after Eq. (22). Inversion of the summations leads to the equivalent and more explicit expression:

$$\begin{aligned} I(t) &= \sum_{i=0}^{vt} (i+1) b_i^{st} + \sum_{i=vt+1}^{+\infty} (vt+1) b_i^{st} \\ &= \sum_{i=0}^{+\infty} (i+1) b_i^{st} + \sum_{i=vt+1}^{+\infty} (vt-i) b_i^{st} \end{aligned} \tag{26}$$

From the knowledge of the steady distribution of polymeric chains b_n^{st} we can thus obtain the dynamical evolution of the global fluorescence in the transient regime (Figure 17).

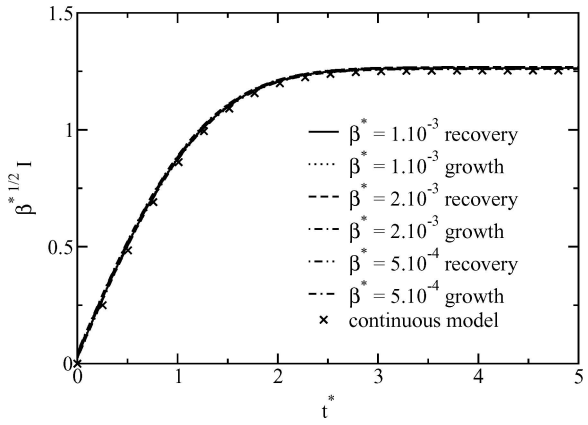

Figure 17. Global fluorescence intensity I as a function of time t^*. Comparison between the signal observed during the growth of the podosome and the signal emitted during the recovery after photo-bleaching for various values of β^*.

As $\beta^* \ll 1$, the continuous model can be used as well. Intensity relaxation after bleaching can be obtained from the discrete model, using the correspondence:

$$I(t^*) \leftrightarrow \sqrt{\beta^*} I^{\text{discrete}}(t)$$

$$I(t^*) = \int_0^{+\infty} x b^{st}(x)\, dx + \int_{t^*}^{+\infty} (t^* - x) b^{st}(x)\, dx$$

Insertion of the steady solution (11) in this expression leads to:

$$I(t^*) = t^* \exp\left[-\frac{t^{*2}}{2}\right] - \int_0^{t^*} x^2 \exp\left(-\frac{x^2}{2}\right) dx$$

which, after integration by part, provides the simple expression:

$$I(t^*) = \int_0^{t^*} \exp\left(-\frac{x^2}{2}\right) dx \tag{27}$$

This last expression could however have been written immediately since it is the generalization of the second equality in Eq. (25). Variations of I are compared to the predictions of the discrete model for various values of β^* in Figure 17.

Thus, the initial fluorescent intensity $I = \sqrt{\pi/2}$ is recovered after a dimensionless typical time $\tau^* = \sqrt{\pi/2}$ [Eq. (27)] corresponding to $\tau = \sqrt{\pi/(2\beta v)}$. Finally, we mention that $I(t)$ also corresponds to the global fluorescent intensity one would measure during the growth of a new podosome. Indeed, since the growth rate v at the basis and the severing rate β of a node do not depend on the length of the podosome, photo-bleaching the podosome is equivalent to cutting it at its basis from

the point of view of fluorescence. A comparison between the global fluorescence intensity during the growth of the podosome and the recovery after photo-bleaching while the podosome is in its steady state shows that the two processes give identical fluorescence signals (Figure 17). Moreover, as the actin cloud surrounding each podosome consists of actin filaments cut from the dense core, the model also accounts for the fact that the recovery of the fluorescence in the cloud occurs with the same characteristic time τ [2].

4.3. Quantitative comparison with the experiments

We described above the structure of an isolated podosome. In clouds, rings, or belts, the podosomes are not isolated, but we can nevertheless try to compare out theoretical results with experimental measurements of the height and life-span of a podosome in order to recover, at least, the order of magnitude of our two parameters β and v.

Indeed, we obtained $h = 2\sqrt{2v/\beta}a$ and $\tau = \sqrt{\pi/(2\beta v)}$, which allow to deduce from experimental $h = 0.5$ μm and $\tau = 30$ s, $\beta \simeq 6.4\ 10^{-4}$ Hz and $v \simeq 2.7$ Hz. We note that, experimentally, the surface area of the bleached region was of about $S = 50\ \mu\text{m}^2$ so that the typical time for the free diffusing monomers to repopulate the bleached region is about $S/D_0 \sim 2$ seconds, much less than τ. Thus, our assumption that the monomers included at the basis of the podosome after bleaching are all fluorescent is valid.

Even if the severing frequency can not be, to our knowlegde, compared to any experimental measurements, we can discuss the value of the polymerization velocity. Indeed, the polymerization frequency $v \simeq 2.7$ Hz is associated to the growth velovity $va \simeq 0.4\ \mu\text{m.min}^{-1}$. Interestingly, this result is in fairly good agreement with measurements of lamellipodial treadmilling in fibroblasts [$0.79 \pm .31\ \mu\text{m.min}^{-1}$, [11]] or of tradmealling in *Listeria* actin comets [8], in regards to the uncertainty in the measurements of h and τ. Moreover, we can expect the spatial extension of the actin cloud around each podosome to be of about $\sqrt{D_0/(8v)} \simeq 1.1$ μm in fairly good agreement with the experimental observations.

On the other hand, from the experimental life-span $\tau_{\text{life}} \simeq 2$ min of a podosome and Eq. (20), we can estimate the concentration of the actin monomers in the hyaloplasm $c_\infty \sim 10\ \mu$M in the case of a podosome consisting of one single actin filament (This last statement comes from the normalization of the distribution b_n to unity). Let us now assume that a podosome consists of an assembly of M filaments. The concentration of the actin monomers in the hyaloplasm that would account for the observed life-span of the podosome must be then divided by M. We know that the gelsolin diffuses freely within the polymeric-actin brush, and thus that the actin filaments do not form a dense structure. Assuming that the distance between two actin filaments is at least twice the size of the actin monomer and taking into account the surface area of the podosome basis, we obtain that M can not be larger 500, leading to $0.02\ \mu\text{M} < c_\infty < 10\ \mu$M. We can only conclude that this

estimation of c_∞ from our model is within the expected range of monomeric-actin concentration in the hyaloplasm. However, we miss experimental data (density of the filament within the podosome and monomeric-actin concentration) that could help validating the model.

5. Conclusion

Introducing two basic ingredients, the continuous polymerization of actin filaments at the basis of the podosome and their equiprobable severing in the whole structure, we account for the apparent shape of the podosome in the confocal microscope and for the characteristic behavior of the fluorescence signal measured in FRAP experiments. Quantitative comparison to the experimental data makes possible to extract from the model the values of the two unknown parameters, v and β, assumed to be constant. Taking into account the diffusion of the fragments cut from the podosome, we are able to explain the existence of the actin cloud surrounding the dense core and the finite life-span of these, at first sight, stationary structures. A dynamical phase diagram is proposed.

The description of the elementary structure, the podosome, is necessary for the understanding of the dynamical behavior of the superstructures, the *clouds*, *rings*, and *belt* that appear during the maturation process of the osteoclasts. Our theoretical results make possible to study the collective behavior of a large set of podosomes which will be the subject of a further publication.

Acknowledgments

The authors would like to thank F. Bard and P. Jurdic for fruitful discussions and reading of the manuscript. We are very grateful to F. Lund for having made possible this collaboration at the Laboratorio de Fisica No Lineal and for many enlightening discussions. This work was supported by Conicyt under Fondap Program N^o 11980002. We also thank the Centre National de la Recherche Scientifique (France) for supporting the research of its members in foreign laboratories.

Appendix I

We derive here the steady solution for the concentration fields of the diffusing species. Let us consider the diffusion Eq. (2), excluding the source term of the second member, in the steady-state (*i.e.* $\frac{\partial}{\partial t} = 0$). The source will be an isolated podosome located at the origin containing M filaments. The concentration fields $c_n(r)$ then satisfy :

$$\frac{1}{1+n}\frac{D_0}{\beta}\Delta_r c_n(r) - n c_n(r) = -2\sum_{i=n+1}^{\infty} c_i(r) \tag{28}$$

Defining $\rho = \sqrt{\beta/D_0}\, r$ and $C_n(\rho) = (D_0/\beta)^{\frac{3}{2}}\, c_n(r)/M$ this equation becomes:

$$\frac{1}{1+n}\Delta_\rho C_n(\rho) - nC_n(\rho) = -2\sum_{i=n+1}^{\infty} C_i(\rho) \tag{29}$$

with the boundary condition in $\rho = 0$:

$$\frac{-2\pi\rho_\sigma^2}{n+1}\left.\frac{\partial C_n(\rho)}{\partial\rho}\right|_{\rho_\sigma} = \sum_{i=n+1}^{+\infty} b_i - \delta_{n,0}\frac{1}{\beta^*}\sum_{i=0}^{+\infty} b_i \tag{30}$$

where $\rho_\sigma = \sqrt{\beta/D_0}\sigma$ is the radius of the hemisphere where the boundary conditions are applied. One must distinguish the cases $n = 0$ and $n > 0$. For $n = 0$, the homogeneous solution reduces to $C_0^h(\rho) = C_\infty/\beta^{*3/2}$, where $C_\infty = (D_0/v)^{3/2}\, c_0(r = +\infty)/M$ stands for the concentration of the monomers far away from the podosome. We chose to normalize this quantity with respect to v rather than β since we expect the growth velocity v to be more easily measured than the depolymerizing frequency β, but this choice is in a large manner arbitrary. For $n > 0$, the homogeneous solution involves the diffusion inverse-length $l_n = \sqrt{n(n+1)}$. The solution to the homogeneous equation, provided that $C_n(\infty) = 0$, writes for a spherically symmetric geometry

$$C_n^h(\rho) = A(n,n)\frac{\exp(-l_n\rho)}{\rho} \quad (\forall n > 0). \tag{31}$$

This solution can be extended to $n = 0$, by noting that $l_0 = 0$ and $A(0,0) = C_\infty/\beta^{*3/2}$. If we now consider the source term, any $C_i(\rho)$ involving the associated diffusion inverse length l_i, we can write the general solution to Eq. (29):

$$C_n(\rho) = \sum_{i=n}^{\infty} A(n,i)\frac{\exp(-l_i\rho)}{\rho} \quad (\forall n \geq 0). \tag{32}$$

Introducing this solution in Eq. (29), one obtains, considering only the coefficient of $\exp(-l_i\rho)/\rho$,

$$-\frac{1}{2}\frac{i(i+1) - n(n+1)}{n+1}A(n,i) = \sum_{j=n+1}^{i} A(j,i) \quad (\forall i > n). \tag{33}$$

The diagonal coefficients $A(n,n)$, which correspond to the solution to the homogeneous equation, are given by the boundary condition. One can use Eq. (33) for expressing any $A(n,i)$ $(i > n)$, as function of the diagonal coefficient $A(i,i)$. One can easily check that applying relation (33) to $i = n+1$ leads to

$$-A(n,n+1) = A(n+1,n+1) \quad (\forall n \geq 0)$$

Let us now denote $\phi(n, i)$, the prefactor of $A(n, i)$ in Eq. (33). Note that $\phi(i, i) = 0$ and $\phi(i, i + 1) = -1$. The difference between the expressions (33) at order $n + 1$ and n leads to

$$\phi(n, i)A(n, i) = [1 + \phi(n + 1, i)]\, A(n + 1, i) \quad (\forall i > n + 1) \tag{34}$$

so that $A(n, n + i) = 0$ for $i \geq 2$ and for all $n \geq 0$. Thus the concentration fields reduce to

$$C_n(\rho) = A(n, n)\frac{\exp(-l_n\rho)}{\rho} - A(n + 1, n + 1)\frac{\exp(-l_{n+1}\rho)}{\rho} \tag{35}$$

where the coefficients $A(i, i)$ are given by the boundary conditions. for $n = 0$ we get:

$$C_0(\rho) = \frac{C_\infty}{\beta^{*3/2}} - A(1, 1)\frac{\exp(-l_1\rho)}{\rho} \tag{36}$$

Note that the stationary solution is physically relevant only if $C_\infty > A(1, 1)\beta^{*\frac{3}{2}} \exp(-l_1\rho_\sigma)/\rho_\sigma$, in order to insure that $C_0(\rho_\sigma) > 0$. In the following, we make use of the boundary condition (30) to determine $A(1, 1)$. The boundary condition writes for $n = 0$:

$$-2\pi(1 + l_1\rho_\sigma)A(1, 1)\exp(-l_1\rho_\sigma) = \sum_{i=1}^{\infty} b_i - \frac{1}{\beta^*}\sum_{i=0}^{\infty} b_i$$

remembering that $l_1 = \sqrt{2}$, $\sum_{i=0}^{+\infty} b_i = 1$ and using the steady expression (4) to derive $b_0 = \beta^*/(1 + \beta^*)$, one finally obtains:

$$A(1, 1) = \frac{1}{2\pi(1 + \sqrt{2}\rho_\sigma)}\,\frac{1}{\beta^*(1 + \beta^*)}\exp(+\sqrt{2}\rho_\sigma)$$

so that:

$$C_0(\rho) = \frac{C_\infty}{\beta^{*\frac{3}{2}}} - \frac{1}{2\pi(1 + \sqrt{2}\rho_\sigma)}\,\frac{1}{\beta^*(1 + \beta^*)}\frac{\exp(-\sqrt{2}(\rho - \rho_\sigma))}{\rho} \tag{37}$$

Appendix II

We present here the derivation of the continuous model in the $\beta^* \to 0$ limit.

THE CONTINUOUS MODEL

Let us use the notations:

$$t^* = \sqrt{\beta v}\, t; \beta^* = \beta/v; \epsilon = \sqrt{\beta^*}; r^* = r/R$$

where R is a length scale that will be specified later. We obtain the following equations after dividing (1), (2) and (3) by $\sqrt{\beta v}$:

$$\begin{aligned}
&\frac{\partial b_n}{\partial t^*} = \frac{b_{n-1} - b_n}{\epsilon} + \epsilon \left[\sum_{i=n+1}^{+\infty} b_i - n b_n \right] \\
&\begin{cases}
\dfrac{\partial c_n(r^*)}{\partial t^*} = \dfrac{1}{\epsilon n + \epsilon} \dfrac{D_0}{R^2 v} \Delta_{r^*} c_n(r^*) + \epsilon \left[2 \displaystyle\sum_{i=n+1}^{+\infty} c_i(r^*) - n c_n(r^*) \right] \\
-\dfrac{D_0}{R^2 v \epsilon (1+n)} \displaystyle\int_{S^*} \nabla_{\mathbf{r}^*} (R^3 c_n(\mathbf{r}^*)) \cdot d\mathbf{S}^* = \epsilon \left[\displaystyle\sum_{i=n+1}^{+\infty} b_i - \delta_{n,0} \frac{1}{\epsilon^2} \sum_{i=0}^{+\infty} b_i \right] \times M
\end{cases}
\end{aligned} \tag{38}$$

While the first equation for b_n has a simple limiting expression when $\epsilon \to 0$, setting $x = \epsilon n$:

$$\frac{\partial b(x)}{\partial t^*} = -\frac{\partial b(x)}{\partial x} + \int_x^{+\infty} b(y)\, dy - x b(x) \tag{39}$$

the second set of equations for c_n is much more complicated due to the singular contribution in $n = 0$. Let us first define R and C_n by:

$$R = \sqrt{D_0/v}; C_n = R^3 c_n / M$$

The new equations for C_n write:

$$\begin{cases}
\dfrac{\partial C_n(r^*)}{\partial t^*} = \dfrac{1}{\epsilon n + \epsilon} \Delta_{r^*} C_n(r^*) + \epsilon \left[2 \displaystyle\sum_{i=n+1}^{+\infty} C_i(r^*) - n C_n(r^*) \right] \\
-\dfrac{1}{\epsilon(1+n)} \displaystyle\int_{S^*} \nabla_{\mathbf{r}^*} (C_n(\mathbf{r}^*)) \cdot d\mathbf{S}^* = \epsilon \left[\displaystyle\sum_{i=n+1}^{+\infty} b_i - \delta_{n,0} \frac{1}{\epsilon^2} \sum_{i=0}^{+\infty} b_i \right]
\end{cases} \tag{40}$$

For $n > 0$ (i.e. $x > 0$) The limiting equations are simply:

$$\begin{cases}
\dfrac{\partial C(x, r^*)}{\partial t^*} = \dfrac{1}{x} \Delta_{r^*} C(x, r^*) + 2 \displaystyle\int_x^{+\infty} C(y, r^*)\, dy - x C(x, r^*) \\
-\dfrac{1}{x} \displaystyle\int_{S^*} \nabla_{\mathbf{r}^*} (C(x, \mathbf{r}^*)) \cdot d\mathbf{S}^* = \displaystyle\int_x^{+\infty} b(y)\, dy; \quad \text{for } x > 0
\end{cases} \tag{41}$$

while for $n = 0$ a careful investigation of the $\epsilon \to 0$ limit is necessary. First it must be noted that $\epsilon \sum_{i=n+1}^{+\infty} C_i$ is the Simpson integral of $C(y)$ for y varying between $x + \epsilon/2$ and $+\infty$. For $x = 0$ the continuous model thus writes:

$$\begin{cases} \dfrac{\partial C(0, r^*)}{\partial t^*} = \dfrac{1}{\epsilon} \Delta_{r^*} C(0, r^*) + 2 \displaystyle\int_{\epsilon/2}^{+\infty} C(y, r^*)\, dy \\ -\dfrac{1}{\epsilon} \displaystyle\int_{S^*} \nabla_{\mathbf{r}^*}(C(0, \mathbf{r}^*)) \cdot d\mathbf{S}^* = \displaystyle\int_{\epsilon/2}^{+\infty} b(y)\, dy - \frac{1}{\epsilon^2} \int_{-\epsilon/2}^{+\infty} b(y)\, dy \end{cases} \tag{42}$$

THE STEADY SOLUTIONS

Equations (39), (41) and (42) can be solved analytically in the steady regime. Equation (39) simply writes, after a differentiation with respect to the variable x:

$$\frac{\partial^2 b^{st}}{\partial x^2} + x \frac{\partial b^{st}}{\partial x} + 2 b^{st} = 0$$

with the boundary conditions that $b^{st}(0) = b^{st}(+\infty) = 0$. One can check that the steady solution writes:

$$b^{st}(x) = x \exp\left(-\frac{x^2}{2} \right) \tag{43}$$

This solution satisfies the normalization condition $\int_0^{+\infty} b^{st}(y) dy = 1$. It must be noted that this prescription implies the following correspondence between the continuous and the discrete model:

$$b(x) \leftrightarrow \frac{b_n}{\sqrt{\beta^*}} \text{ where } x = \sqrt{\beta^*} n \tag{44}$$

Equation (41) for the concentration profiles can be rewritten as:

$$\Delta_{r^*} C^{st}(x, r^*) - x^2 C^{st}(x, r^*) = -2x \int_x^{+\infty} C^{st}(y, r^*)\, dy \tag{45}$$

for $r^* > r_\sigma^* \equiv \sigma / \sqrt{D_0 / v}$ and $x > 0$, with the boundary condition in $r^* = r_\sigma^*$:

$$-2\pi r_\sigma^{*2} \left. \frac{\partial C^{st}(x, r^*)}{\partial r^*} \right|_{r_\sigma^*} = x \int_x^{+\infty} b^{st}(y)\, dy \quad (x > 0) \tag{46}$$

One can check that a solution of the type

$$C^{st}(x, r^*) = [A(x) r^* + B(x)] \frac{\exp(-x r^*)}{r^*}$$

satisfies (45) provided

$$A(x)\exp(-xr^*) = \int_x^{+\infty} [A(y)r^* + B(y)]\exp(-yr^*)dy$$

which, after a differentiation with respect to x leads to $B(x) = -A'(x)$, the prime denoting a derivation with respect to x. Inserting $C^{st}(x, r^*) = [A(x)r^* - A'(x)]\exp(-xr^*)/r^*$ in the boundary condition (46) with b^{st} given by (43), and assuming $A(x = +\infty) = 0$, we finally get:

$$A(x) = \frac{\exp(-x^2/2 + r_\sigma^* x)}{2\pi(1 + r_\sigma^* x)} \tag{47}$$

and thus:

$$C^{st}(x, r^*) = \left[1 - \frac{\left(r_\sigma^{*2} - 1\right)x - r_\sigma^* x^2}{(1 + r_\sigma^* x)r^*}\right] \frac{\exp(-x(r^* - r_\sigma^*) - x^2/2)}{2\pi(1 + r_\sigma^* x)} \quad (x > 0) \tag{48}$$

The same prescription can be used to solve the $x = 0$ case, the steady equation is now:

$$\Delta_{r^*} C^{st}(0, r^*) = -2\epsilon \int_{\epsilon/2}^{+\infty} C^{st}(y, r^*)\, dy$$

However, inserting the $\epsilon \to 0$ solution (48) in the RHS does not provide the correct solution, it simply leads to an inconsistency. To obtain the proper solution, one must solve the full equation for all values of x at the same order in ϵ . We will see that for $x > 0$ the $\epsilon \to 0$ limit corresponds to (48) , as expected. The full steady equation writes for finite ϵ:

$$\Delta_{r^*} C^{st}(x, r^*) - x(x + \epsilon)C^{st}(x, r^*) = -2(x + \epsilon) \int_{x+\epsilon/2}^{+\infty} C^{st}(y, r^*)\, dy \tag{49}$$

with the boundary condition:

$$\begin{aligned} -2\pi r_\sigma^{*2} \left.\frac{\partial C^{st}(x, r^*)}{\partial r^*}\right|_{r_\sigma^*} &= (x + \epsilon) \int_{x+\epsilon/2}^{+\infty} b^{st}(y)\, dy \quad (x > 0) \\ -2\pi r_\sigma^{*2} \left.\frac{\partial C^{st}(0, r^*)}{\partial r^*}\right|_{r_\sigma^*} &= \epsilon \int_{\epsilon/2}^{+\infty} b^{st}(y)\, dy - \frac{1}{\epsilon} \int_{-\epsilon/2}^{+\infty} b^{st}(y)\, dy \end{aligned} \tag{50}$$

Guided by the discrete model, the generic solution for (49) can be searched of the form :

$$C^{st}(x, r^*) = \frac{1}{\epsilon r^*}[A(x)\exp(-\sqrt{x(x+\epsilon)}r^*) + B(x+\epsilon)\exp(-\sqrt{(x+\epsilon)(x+2\epsilon)}r^*)] \quad (51)$$

Insertion of this expression in (49) leads to:

$$B(x+\epsilon)\exp\left(-\sqrt{(x+\epsilon)(x+2\epsilon)}r^*\right) = -\int_{x+\epsilon/2}^{+\infty} C^{st}(y, r^*)\, dy$$

differentiation with respect to x gives the compatibility condition:

$$\frac{\partial}{\partial x}[B(x+\epsilon)\exp\left(-\sqrt{(x+\epsilon)(x+2\epsilon)}r^*\right)] = C^{st}(x+\epsilon/2, r^*)$$

which is only true when $\epsilon \to 0$ if $B(x) = -A(x)$. We thus obtain that

$$C(x, r^*) = \frac{1}{\epsilon r^*}[A(x)\exp\left(-\sqrt{x(x+\epsilon)}r^*\right) - A(x+\epsilon)\exp\left(-\sqrt{(x+\epsilon)(x+2\epsilon)}r^*\right)] \quad (52)$$

This solution also holds in $x = 0$, the first term is simply replaced by an arbitrary constant (proportional to the monomer concentration $C_\infty = (D_0/v)^{\frac{3}{2}}\, c_0(r = +\infty)/M$, far away from the podosome). When $x > 0$, The boundary condition in r_σ^* simply gives back (47) in the $\epsilon \to 0$ limit, and the steady solution (48) is recovered. When $x = 0$, the solution rewrites:

$$C(0, r^*) = \frac{C_\infty}{\sqrt{\beta^*}} + B\frac{\exp(-\sqrt{2}\epsilon r^*)}{r^*}$$

where we have used the correspondence $C(0, r^*) \leftrightarrow (D_0/v)^{3/2}\, c_0/\sqrt{\beta^*}/M$, and B is determined by the boundary condition in r_σ^* (50):

$$2\pi B(1+\sqrt{2}\epsilon r_\sigma^*)\exp(-\sqrt{2}\epsilon r_\sigma^*) = \epsilon \exp\, g\left(-\frac{\epsilon^2}{8}g\right) - \frac{1}{\epsilon}\exp\left(-\frac{\epsilon^2}{8}\right)$$

which at the leading order writes $B \sim -\exp(-\sqrt{2}\epsilon r_\sigma^*)/(2\pi\epsilon)$. Recalling that $\epsilon = \sqrt{\beta^*}$ we deduce:

$$C(0, r^*) \sim \frac{C_\infty}{\sqrt{\beta^*}} - \frac{1}{2\pi\sqrt{\beta^* r^*}}\exp\left(-\sqrt{2\beta^*}(r^* - r_\sigma^*)\right) \quad (53)$$

Appendix III

In this part we prove that expression (14) satisfies Eq. (8). First it is useful to rewrite $b(t^*, x)$ as:

$$b(t^*, x) = b^{st}(x)\theta(t^* - x) + \delta(x - t^*) \int_{t^*}^{+\infty} b^{st}(x)\, dx \tag{54}$$

where $\theta(x)$ is the Heaviside step function. We can easily check that this solution is normalized. To check whether (8) is satisfied, it is interesting to introduce a generic auxiliary function $\psi(x)$ satisfying $\psi(0) = \psi(+\infty) = 0$, and to consider the action of the two members of (8) on ψ. The left member writes:

$$L \equiv \int_0^{+\infty} \frac{\partial b(t^*, x)}{\partial t^*} \psi(x)\, dx = \frac{\partial}{\partial t^*} \left(\int_0^{+\infty} b(t^*, x)\psi(x)\, dx \right)$$

Insertion of (54) leads to

$$L = \frac{\partial}{\partial t^*} \left(\int_0^{t^*} b^{st}(x)\psi(x) + \psi(t^*) \int_{t^*}^{+\infty} b^{st}(x)\, dx \right)$$

which, after differentiation leads to:

$$L = \left. \frac{\partial \psi}{\partial x} \right|_{x=t^*} \int_{t^*}^{+\infty} b^{st}(x)\, dx \tag{55}$$

The right member of (8) writes:

$$\begin{aligned} R &\equiv \int_0^{+\infty} \left[-\frac{\partial b}{\partial x}\psi(x) + \psi(x) \int_x^{+\infty} b(y)dy - x\psi(x)b(x) \right] dx \\ &= -[b(t^*, x)\psi(x)]_0^{+\infty} + \int_0^{+\infty} b(t^*, x)\frac{\partial \psi}{\partial x} \\ &\quad + \int_0^{+\infty} \psi(x) \left(\int_x^{+\infty} b(t^*, y)dy \right) dx - \int_0^{+\infty} x\psi(x)b(x)\, dx \end{aligned} \tag{56}$$

The integrated term cancels thanks to the conditions $\psi(0) = 0$ and $\psi(+\infty) = b(t^*, +\infty) = 0$, and the second term writes, after usage of (54):

$$\int_0^{+\infty} b(t^*, x)\frac{\partial \psi}{\partial x} = \int_0^{t^*} b^{st}(x)\frac{\partial \psi}{\partial x}\, dx + \left. \frac{\partial \psi}{\partial x} \right|_{x=t^*} \int_{t^*}^{+\infty} b^{st}(x)\, dx$$

Integration by parts of the first term leads to:

$$\int_0^{+\infty} b(t^*, x)\frac{\partial \psi}{\partial x} = b^{st}(t^*)\psi(t^*) - \int_0^{t^*} \psi(x)\frac{\partial b^{st}}{\partial x}\, dx + L$$

The third term of (56) writes:

$$\int_0^{+\infty} \psi(x) \left(\int_x^{+\infty} b(t^*, y)\, dy \right) dx = \int_0^{+\infty} \psi(x) \left(\int_x^{t^*} b^{st}(y)\, dy + \int_{t^*}^{+\infty} b^{st}(y)\, dy \right) \theta(t^* - x)\, dx \tag{57}$$

or equivalently

$$\int_0^{+\infty} \psi(x) \left(\int_x^{+\infty} b(t^*, y)\, dy \right) dx = \int_0^{t^*} \psi(x) \left(\int_x^{+\infty} b^{st}(y)\, dy \right) dx$$

The last term of (56) becomes:

$$\int_0^{+\infty} x\psi(x) b(x) dx = \int_0^{t^*} x\psi(x) b^{st}(x) dx + t^* \psi(t^*) \int_{t^*}^{+\infty} b^{st}(x)\, dx$$

Inserting all these results in (56) leads to:

$$R = L + \psi(t^*) \left[b^{st}(t^*) - t^* \int_{t^*}^{+\infty} b^{st}(x) dx \right] + \int_0^{t^*} \psi(x) \left(-\frac{\partial b^{st}}{\partial x} + \int_x^{+\infty} b^{st}(y)\, dy - x b^{st}(x) \right) dx \tag{58}$$

Since $b^{st}(x)$ is the steady solution of (8) the last term cancels, and from $b^{st}(x) = x \exp(-x^2/2)$ one can easily check that the second term also cancels, so that we end up with $R = L$, proving that Eq. (8) is satisfied by (14).

References

1. Chellaiah, M., Kizer, N., Silva, M., Alvarez, U., Kwiatkowski, D. and Hruska, K.A. Gelsolin deficiency blocks podosome assembly and produces increased bone mass and strength. *J. Cell Biol.* **148** (2000), 665–678.
2. Destaing, O., Saltel, F., Géminard, J.-Ch., Jurdic, P. and Bard, F. Podosomes Display Actin turnover and Dynamic Self-Organization in Osteoclasts Expressing Actin-Green Fluorescent Protein. *Mol. Biol. Cell* **14** (2003) 407–416.
3. Einstein, A. ber die von der molekularkinetischen Theorie der Wrme geforderte Bewegung von in ruhenden Flssigkeiten suspendierten Teilchen. *Ann. Phys.* **17** (1905), 549.
4. Gavazzi, I., Nermut, M.V. and Marchisio, P.C. Ultrastructure and gold-immunolabelling of cell-substratum adhesions (podosomes) in RSV-transformed BHK cells. *J. Cell Sci.* **94** (1989), 85–89.
5. Marchisio, P.C., Cirillo, D., Naldini, L., Primavera, M.V., Teti, A. and Zambonin-Zallone, A. Cell-substratum interaction of cultured avian osteoclasts is mediated by specific adhesion structures. *J. Cell Biol.* **99** (1984), 1696–1705.

6. Marchisio, P.C., Cirillo, D., Teti, A., Zambonin-Zallone, A. and Tarone, G. Rous sarcoma virus-transformed fibroblasts and cells of monocytic origin display a peculiar dot-like organization of cytoskeletal proteins involved in microfilament-membrane interactions. *Exp. Cell Res.* **169** (1987), 202–214.
7. Nermut, M.V., Eason, P., Hirst, E.M. and Kellie, S. Cell/substratum adhesions in RSV-transformed rat fibroblasts. *Exp. Cell Res.* **193** (1991), 382–397.
8. Pantaloni, D., Le Clainche, C. and Carlier, M.F. Mechanism of actin-based motility. *Science* **292** (2001), 1502–1506.
9. Pfaff, M. and Jurdic, P. Podosomes in osteoclasts-like cells: structural analysis and cooperative roles of paxillin, proline-rich tyrosine kinase 2 (Pyk2) and integrin $\alpha V\beta 3$. *J. Cell Sci.* **114** (2001) 2775–2786.
10. Tarone, G., Cirillo, D., Giancotti, F.G., Comoglio, P.M. and Marchisio, P.C. Rous sarcoma virus-transformed fibroblasts adhere primarily at discrete protusions of the ventral membrane called podosomes. *Exp. Cell Res.* **159** (1985) 141–157.
11. Wang, Y.L. Exchange of actin subunits at the leading edge of living fibroblasts: possible role of treadmilling. *J. Cell Biol.* **101** (1985), 597–602.